Available online at www.sciencedirect.com
ScienceDirect
Estuarine, Coastal and Shelf Science 76 (2008) 153–162
ESTUARINE COASTAL AND SHELF SCIENCE
www.elsevier.com/locate/ecss

Spatial and temporal variation of picoplanktic cyanobacteria population in a density stratified estuary, and the introduction of a cellular gradient number

Alejandro Carrillo [a,b], Pablo Huq [b,*], Mari C. Pérez [c], José M. Redondo [a]

[a] *Departamento de Física Aplicada, Universitat Politècnica de Catalunya, Jordi Girona 1-3, Campus Nord-UPC, Mòdul B4-B5, 08034 Barcelona, Spain*
[b] *College of Marine and Earth Studies, University of Delaware, Newark, DE 19716, USA*
[c] *Universidad Politécnica de Valencia, Spain*

Received 13 April 2005; accepted 8 June 2007
Available online 27 September 2007

Abstract

Spatial and temporal variations in the distribution of the marine picoplanktic cyanobacteria population and mixing conditions were found in the Ebro River estuary outflow to the Mediterranean Sea in Spain. Six sampling surveys were undertaken between July 1999 and February 2000 for distances up to 15 km from the river mouth. Measurements were taken of flow velocity, salinity, temperature, depth and picocyanobacteria (PCB) abundances. Gradient Richardson (Rig) and Reynolds (*Re*) numbers were determined to evaluate hydrodynamics. In summer, large values of Rig arise from the small flow rates, and small values of velocity shear between the surface fresh water layer and the bottom saline layer; conversely, in winter the large flow rates and attendant large velocity shears between the layers give rise to small values of Rig. Flow conditions in the fall are an intermediate case between the summer and winter cases. Vertical abundance distributions were resolved through the river water, interfacial region, and the bottom salt wedge; longitudinal gradients of PCB abundances were also resolved. Seasonal differences in the PCB abundance values were observed. Analysis of cell numbers (C) showed that the variable dC/dS, the dependence of cell number upon salinity gradient (dS) was critical. A non-dimensional number; the cellular gradient number (Cg) is introduced. Cg has useful biological interpretations that can potentially be included in ecological modeling. For example, $Cg = 1$ pertains to perfect adaptability of the organism to adjust to changing environmental conditions, whereas $Cg = 0$ describes total mortality. For a system with strong advection there is insufficient time for cells to adapt to the changing environment, and so those cell counts are unchanged. This is the case for the Ebro estuary in winter as advection of salinity (and hence PCB abundance) dominates the other loss processes for large flow rates.

Keywords: phytoplankton; picocyanobacteria; river; estuaries; mixing; stratified flows; salinity gradients

1. Introduction

It is important to assess the impacts of increasing pollution on the estuarine environment. This is because estuarine environments are areas of feeding, growth and reproduction for complex organisms due to its rich waters, and so is a location that provides critical input into the base of the food web (Islam and Tanaka, 2004). Modeling of impacts is difficult as it requires understanding of coupling between hydrodynamic and biological processes; the difficulty is compounded by the inherent temporal and spatial variability of both the hydrodynamics as well as the biological fields. An important first step is to understand the coupling between hydrodynamics and biology. There is, however, a lack of data that relate biological and hydrodynamic measurements. The objective of this paper is to determine the role of salinity upon picocyanobacteria abundances in the estuary of the Ebro River in north-eastern Spain. The magnitudes of tides are small in rivers out-flowing to the

* Corresponding author.
E-mail address: huq@udel.edu (P. Huq).

0272-7714/$ - see front matter © 2007 Elsevier Ltd. All rights reserved.
doi:10.1016/j.ecss.2007.06.015

Mediterranean Sea. Typically estuaries in the Mediterranean Sea are stratified with a wedge of relatively dense (saline) water penetrating upstream under the out-flowing river water in such estuaries. A density interface exists between the fresh and saline waters, and the extent of the upstream penetration of the saline wedge is dependent upon the river flow magnitudes (Perkins, 1976).

The work described is part of the PIONEER project (European Project at the Ebro River estuary), and the results presented in this paper are part of a more extensive study of the phytoplankton ecology in the lower Ebro River. We report on the abundances of picoplankton for a distance of 15 km upstream from the river mouth. It was found that the picoplankton is composed of minute chroococcoid cyanobacteria and eukaryotic phytoplankton cells. The abundance of picoplankton has been measured in estuarine studies (e.g. Ray et al., 1989; Iriarte, 1993; Sin et al., 2000). Here the contribution of picoplankton to the total aquatic net primary producers is at least 10% (Raven, 1998). This affirms the role of picoplankton as an integral component of the microbial food web (Sieburth et al., 1978). Fluctuations in nutrient concentration levels, temperature or light can result in seasonal variations of 2–3 orders of magnitude in picoplankton cyanobacteria abundance in coastal and shelf ecosystem; in contrast, in the open ocean variations in abundance generally only vary by a factor of approximately 2 (Chiang et al., 2002). Pérez and Carrillo (2005) analyzed the same phytoplankton fraction, picoplankton cyanobacteria (PCB), as in this work and found a direct relationship between salinity and PCB abundances, and also that the fresh water values for PCB were zero.

We report measurements of the spatial (vertical and longitudinal) and temporal (seasonal) variations of PCB abundances in the Ebro River estuary. Section 2 describes the location of the study area, and presents information of the sampling methodology, as well as the hydrodynamic or flow magnitudes. Section 3 presents results distinguishing the role of salinity from those conditions controlled mainly by the river flow. The relationship between salinity and PCB abundances is discussed in Section 4. Our observations suggest that PCB abundances are dependent upon the salinity gradient, and we introduce a biotic index – a cellular gradient number – to relate hydrodynamics and biology measurements.

2. Materials and methods

2.1. Study area

The area comprises the lower part of the Ebro River – the last 15 km – from Gracia Island to its mouth in the Mediterranean Sea (Fig. 1). It is located in the north-west of the Mediterranean Sea in northern Spain close to the border between Spain and France between 40°40′ N and 00°40′ E. The Ebro River is 960 km in length, and has a drainage area of 88,835 km^2, and is one of the main rivers in Spain with several dams that control the river flow (Ibáñez et al., 1999). In general, low rainfall in the summer results in small river flows (approximately 100 m^3 s^{-1}),

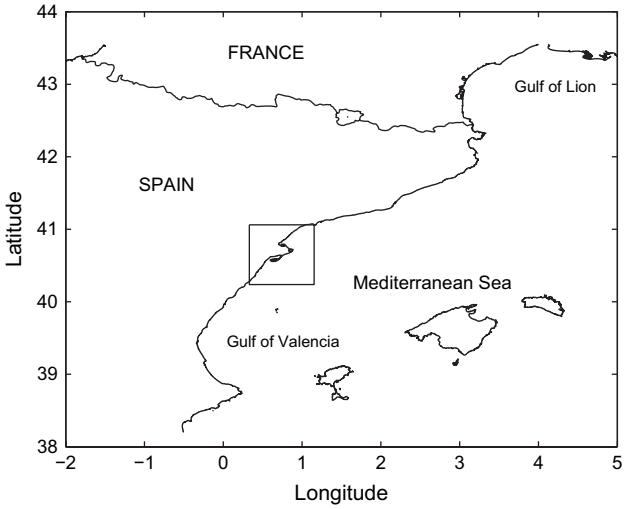

Fig. 1. Study area of the Ebro River in north-eastern Spain.

whereas high rainfall in the winter results in larger river flows (approximately 450 m^3 s^{-1}). Suspended inert solid's concentration conditions are usually low. The region has a dry Mediterranean climate with a mean annual temperature of around 16–17 °C, and approximately 550 mm of rainfall per year (Martínez et al., 1999). Experimental measurements were taken in the summer, fall and winter between July 8 and 12, October 5 1999, and February 3 and 5 2000, respectively.

2.2. Sampling

Water samples were taken in the water column at six sampling stations (Fig. 2). At each station, 10 water samples were taken at different depths; four samples were located at fixed depths (surface and 1.5, 3 and 4.5 m below the

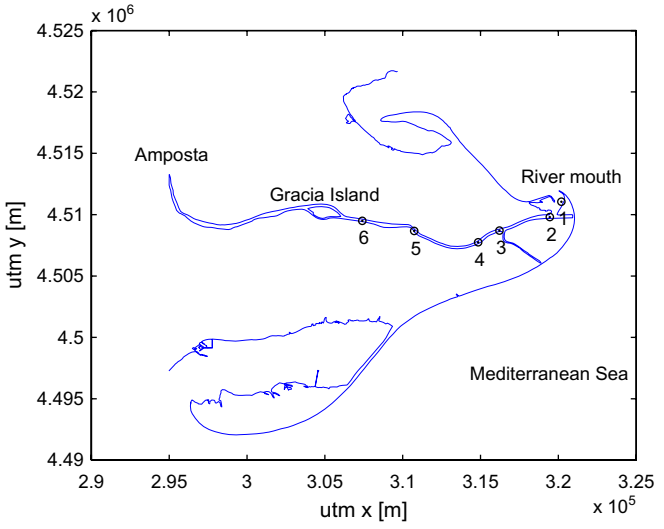

Fig. 2. Map of the six fixed seasonally sampled stations on the last 15 km of the Ebro River.

surface), and a further six samples were obtained deep in the fluid column of the river (and through the fresh water–sea water interface).

Temperature and salinity (Practical Salinity Scale) were measured with a Seabird CTD and a Hydrolab Surveyor 3 multiparametric probe, and velocity was measured with an ADP Nortek. The water samples were taken using a pump with the hose located at the depth selected by the Hydrolab. The Hydrolab can measure temperatures between −5 and 50 °C (accuracy ±0.10 °C), specific conductivity between 0 and 100 mS m^{-1} (accuracy ±1%) and depths between 0 and 100 m (accuracy ±0.1 m). The ADP was calibrated in shallow waters, and can measure in a depth range between 0 and 6 m with a resolution of 0.20 m; the minimum distance to the first depth of 0.4 m. The velocity range was ±10 m s^{-1}, velocity resolution ±0.1 cm s^{-1}) and maximum sampling rate of 0.5 Hz. Velocity time series was averaged over 20 s.

Phytoplankton samples for qualitative and quantitative analyses were collected in bottles at each depth. The material was fixed in situ with glutaraldehyde (2% final concentration) according to Sournia (1978). A slide was prepared from each sample by filtering 10 or 20 ml of water, depending on phytoplankton concentration, onto 0.2 μm Millipore membrane filters. Under blue light excitation, cyanobacterial cells fluoresced yellow-orange. The cell counts were done by epifluorescence microscopy (Vargo, 1978) using a Nikon Optiphot microscope equipped with a mercury lamp, using 100× oil-immersion objective. A minimum of 300 cells were counted and at least 100 cells of the more abundant species with an error less than 20% in accord with Lund et al. (1958).

2.3. Non-dimensional parameters

Results are presented in a coordinate system where the x-axis is in the direction of the river flow, the y-axis is orthogonal to the river flow and the z-axis indicates depth. A schematic of the fresh water river flow separated by a density interface above the intruding salt water wedge is presented in Fig. 3. The interface begins at depth D, and the end of the interface occurs at depth $D + h$ so that the interface or mixing layer thickness is h.

2.3.1. River flow

The river flow (Q) is calculated by:

$$Q = Au \tag{1}$$

where A is the cross sectional area and u is the mean velocity of the river.

2.3.1.1. Gradient Richardson number. The buoyancy frequency ($N^2 = -g/\rho_0(\mathrm{d}\rho/\mathrm{d}z)$) of the density gradient ($\mathrm{d}\rho/\mathrm{d}z$) is related to the strength of the buoyancy force; the magnitude of the inertial forces is related to the velocity gradient. The relative balance between buoyancy and inertial forces, expressed by the ratio of the square of the buoyancy frequency N and the velocity gradient ($\mathrm{d}u/\mathrm{d}z$), is the gradient Richardson number Rig. It is known that the vertical mixing rates decrease with increasing Rig (Turner, 1973), where Rig is formally given by:

$$\mathrm{Rig} = \frac{N^2}{\left(\frac{\mathrm{d}u}{\mathrm{d}z}\right)^2} = \frac{-g}{\rho_0}\frac{\frac{\mathrm{d}\rho}{\mathrm{d}z}}{\left(\frac{\mathrm{d}u}{\mathrm{d}z}\right)^2} \tag{2}$$

where u denotes the mean velocity, g the gravitational acceleration, ρ and ρ_0 denoted the mean density and the mean density in the middle of the mixing layer, respectively. The gradients $\mathrm{d}\rho/\mathrm{d}z$ and $\mathrm{d}u/\mathrm{d}z$ occur across the interface or mixing layer.

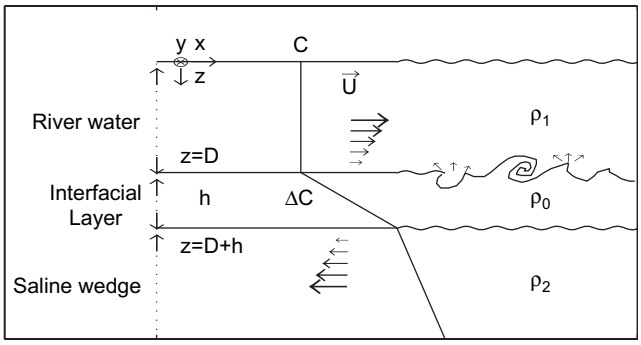

Fig. 3. Vertical section of the estuary showing a three-layer structure of river water in the topmost layer, an interfacial layer in the middle, and a bottom saline wedge. The symbols C, U and ρ are cell number, velocity and water density, respectively. The x-axis is in the direction of the upper layer river flow, the y-axis is orthogonal to the river flow, and z-axis indicates depth. Indicated in the figure is an interfacial layer of thickness h; cell number, velocity and density vary through the depth of the interfacial layer.

2.3.1.2. Reynolds number. The Reynolds number relates the relative magnitudes of inertial to viscous forces. Formally:

$$Re = \frac{uD}{\nu} \tag{3}$$

where u and D are velocity and scale characteristics of the flow and ν is the kinematic viscosity of the fluid.

3. Results

3.1. Values of the hydrodynamical parameters Re and Rig for the Ebro River

Values of flow rates for summer, fall and winter were 114 m^3 s^{-1} (July 12) and 184 m^3 s^{-1} (July 8), 282 m^3 s^{-1} (October 6), 635 m^3 s^{-1} (February 5) and 900 m^3 s^{-1} (February 3). These correspond to values of Re on July 8 of 4×10^4 and 1.3×10^5; 10^4 and 2×10^5 for July 12; 1.3×10^5 and 7×10^5 for October 6 and February 5. Values of flow rates, velocities, PCB, salinities, temperature and each of the three layers in the estuary (river or fresh water layer at the surface, mixing layer at the interface and the sea or saline layer at the bottom) are tabulated in Table 1.

Table 1
Compendia of the mean values from the sampled day of July 8 and 12, October 5 and 6, February 3 and 5. Data from flow ($\overline{Q}$) and standard flow deviation ($\overline{\sigma Q}$) corresponded to the river water layer. Data from velocity (u), PCB counts ($\overline{\text{PCB}}$), salinity and temperature corresponded to the river water layer (R), mixing layer (M) and sea water layer (S). The boundaries (begin and end) and thickness h of the interface is also presented

Date	$\overline{Q}$ [$m^3 s^{-1}$]	$\overline{\sigma Q}$ [$m^3 s^{-1}$]	u [$m s^{-1}$]		$\overline{\text{PCB}}$[cell (L^{-1})$\times 10^7$]			Salinity [psu]			Temperature [°C]			Interface [m]		
			R	S	R	M	S	R	M	S	R	M	S	begin	end	$\overline{h}$
July 8	184	81	0.20	0.02	0.99	1.83	5.30	2.7	19.9	34.1	25.8	24.9	24.3	1.6	2.7	1.1
July 12	114	30	0.41	0.32	0.58	3.14	6.22	2.5	21.3	34.7	26.9	25.2	23.7	1.3	2.2	0.9
October 5	No data		0.36	0.29	1.24	3.35	13.8	2.6	21.7	35.1	No data					
October 6	282	101	0.40	0.14	1.01	3.84	18.9	3.3	22.8	35.4	20.9	22.0	22.1	3.0	4.6	1.6
February 3	900	642	0.75	0.01	No wedge			0.4	No wedge		9.9	No wedge				
February 5	635	412	0.64	0.17	0.24	4.17	9.18	0.4	16.0	33.0	10.1	9.1	9.8	4.6	5.8	1.2

Values of the hydrodynamical quantities, expressed in terms of the non-dimensional parameters, the Reynolds number (Re) and the gradient Richardson number (Rig) are useful to facilitate comparisons. The measured data show that Rig $\propto Re^{-3/2}$ in Fig. 4. In summer, large values of Rig arise from the small flow rates, and small values of velocity shear between the surface fresh water layer and the bottom saline or sea water layer; conversely, in winter the large flow rates and attendant large velocity shears between the layers give rise to small values of Rig. Flow conditions in the fall are an intermediate case between the summer and winter cases. No saline wedge intrusions were observed for large flow rates where the value of the Re numbers were greater than 10^6.

3.2. Saline wedge variability

Out-flowing fresh water of depth D is separated by a salinity interface of thickness h above the bottom saline wedge. Values of salinity were 0.4 and 35.4 psu at the top and bottom of the interface. The longitudinal variation at the center of the interface ($D + h/2$) is shown in Fig. 5. Upstream values of ($D + h/2$) are greater with measured values between 2.5 and 8.7 m below the surface, whereas at the river mouth values ranged between 1 and 4 m. The depth of the center of the interface is dependent on the river flow and thus there is also a seasonal variation. It is evident in Fig. 5 that interfacial depths are greatest in the winter and smallest in the summer.

3.3. Vertical distributions of picoplankton cyanobacteria abundance

Vertical profiles of PCB abundance at each of the six stations in the estuary are presented in Fig. 6 for summer, fall and winter. The vertical axis is depth and the horizontal axis is abundance in this figure. Abundances are small near

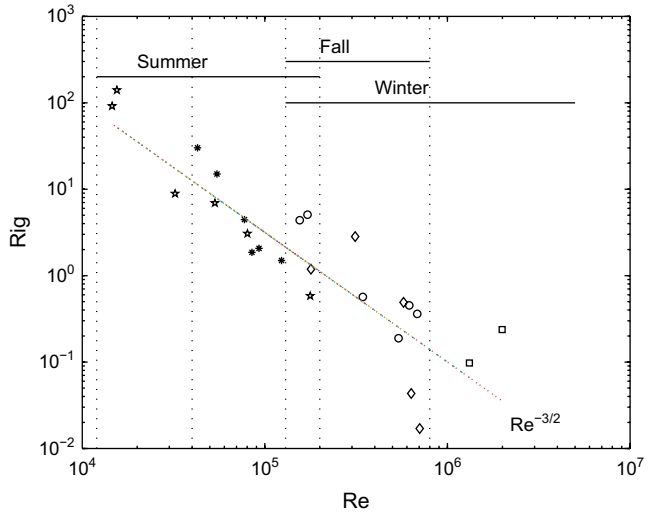

Fig. 4. The parameter space Rig–Re of the estuary for summer, fall and winter. Data for July 8 (*) and 12 (☆), October 6 (○), and February 3 (□) and 5 (◇). A best-fit line Rig $\approx Re^{-3/2}$ is fitted through the data.

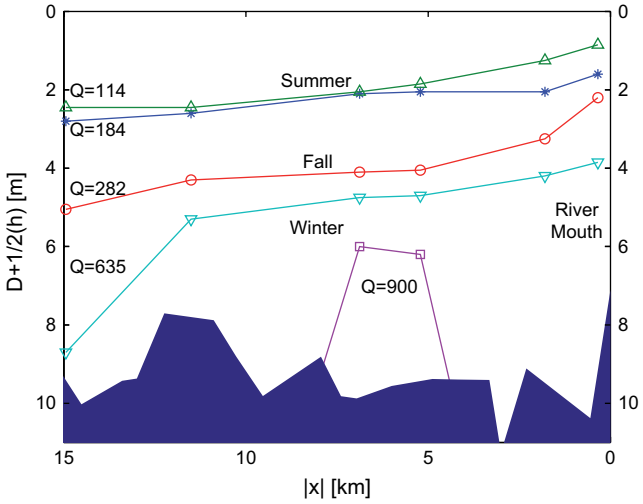

Fig. 5. Plot showing the longitudinal evolution of the middle of the interface ($D + h/2$) in the estuary, for summer, fall and winter.

the surface and greatest close to the bottom of the river. The figure shows the main changes in abundances occurred at the interface (delineated by horizontal lines) and its vicinity. Abundances varied in the different layers, smallest values ($0.1 < \text{cell } (L^{-1}) < 5 \times 10^6$) were found in the fresh upper layer; the interfacial layer possesses intermediate values ($0.2 < \text{cell } (L^{-1}) < 1.6 \times 10^7$); and highest abundance values ($0.2 < \text{cell } (L^{-1}) < 3 \times 10^7$) occur in the bottom saline wedge. A one-way ANOVA variance analysis (probability $P < 0.05$) shows that the difference between abundances in the different layers was significant, whereas there were no significant differences ($P > 0.05$) within each layer. There is also a seasonal variation of abundance in Fig. 6 between summer, fall and winter; however, the seasonal variation is more evident in Fig. 7.

3.4. Seasonal variation of distributions of picoplankton cyanobacteria abundance

For each layer, the average value of abundance in the layer was determined from the total abundance of all six stations (R1–R6). Data were collected on 2 days in each season (8 and 12 July, 5 and 6 October, 3 and 5 February) to determine seasonal variability (summer, fall and winter). Fig. 7 shows that the abundance of picoplanktic cyanobacteria increases from summer to fall, and decreases from fall to winter in both upper fresh water and lower brackish water layers.

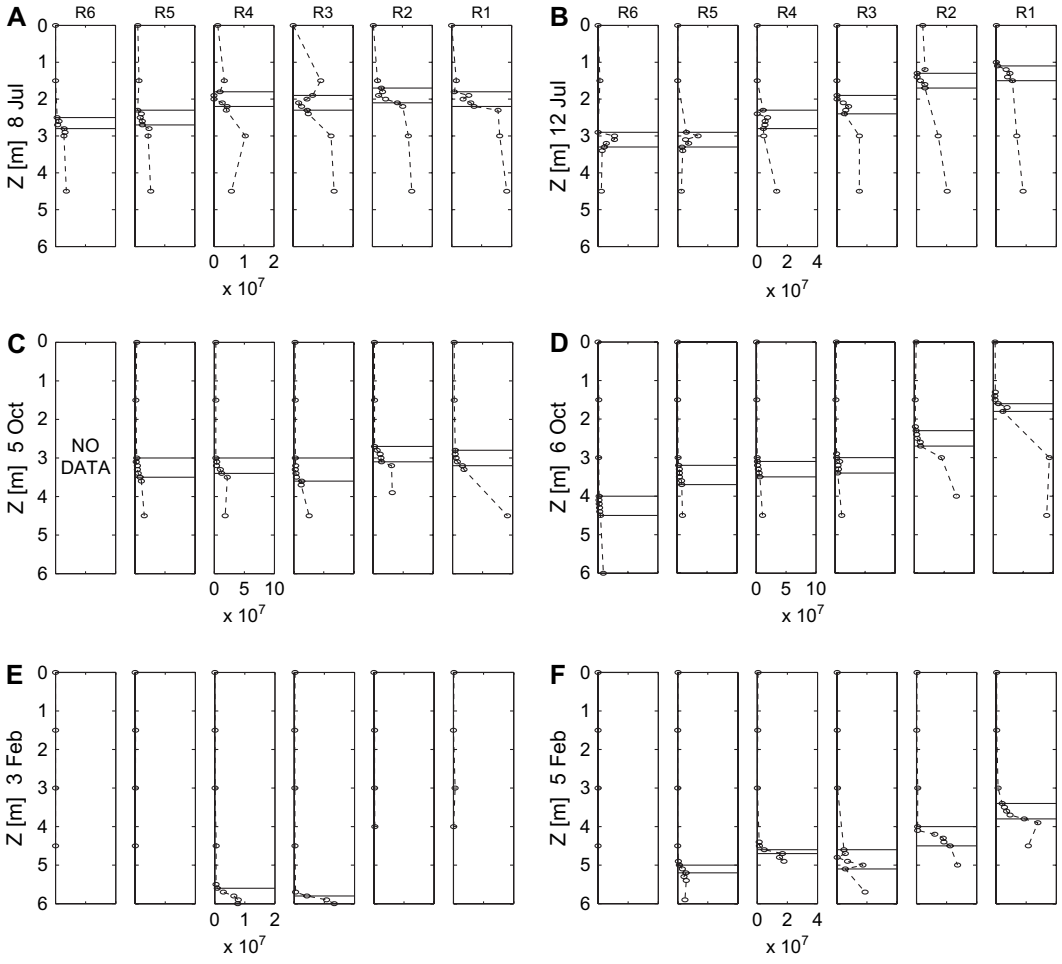

Fig. 6. Plot showing the vertical profiles of cell number (PCB abundances) with depth in the estuary for each of the six stations; for July 8 (A) and 12 (B), October 5 (C) and 6 (D), February 3 (E) and 5 (F). Horizontal lines show the beginning and the end of the interface in each station.

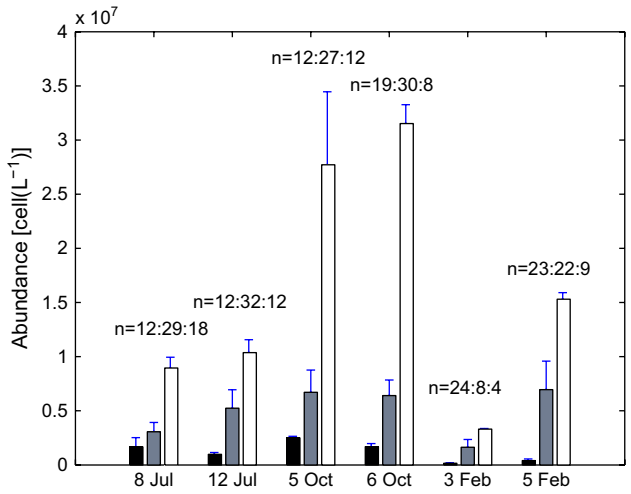

Fig. 7. Averaged abundance or population of picoplanktic cyanobacteria (PCB) – data from July 8 and 12, October 5 and 6 and February 3 and 5. Upper, interface and saline layers are shown in black, grey and white bars; n is the number of water samples analyzed in each layer. Error bars are also shown.

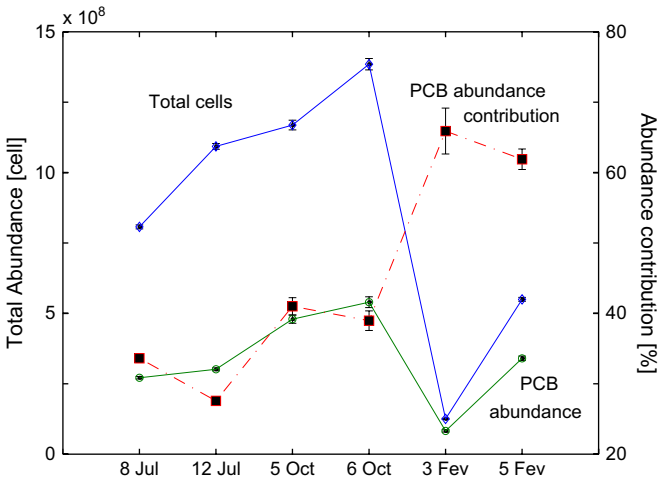

Fig. 8. Seasonal variation of the integrated cell numbers through the water column. The ordinate for total cell number (◇) and PCB abundance (○) is given by the left hand scale. PCB abundance contribution to the total phytoplankton (■) is given by the right hand ordinate. Error bars are shown.

Averaged abundance values for summer, fall and winter were 9.7×10^5, 1.6×10^6, 4.03×10^5 and 1.03×10^7, 3.15×10^7, 1.5×10^7 for the upper and lower layers, respectively. Values of the abundance for the interfacial layer were 5.2×10^6, 6.4×10^6, 6.9×10^6 for summer, fall and winter. A one-way ANOVA variance analysis ($P > 0.05$) showed that there were no significant differences between the results of summer (July 8 and 12) and fall (October 5 and 6), however, the differences in winter (February 3 and 5) were significant ($P < 0.05$). This was due to the absence of a saline wedge on February 3.

The fresh water value for PCB abundance is zero, and the maximum PCB abundance value of 93.7×10^6 cell (L^{-1}) was measured in the saline layer at the mouth of the estuary in October 6 at a depth of 3 m. Additionally we also integrate the total phytoplankton (including PCB) in the water column and PCB values. Fig. 8 shows the seasonal variation for total phytoplankton, the total PCB abundances and the PCB fraction of the total abundance. The minimum value of PCB abundance (8.2×10^7 cell (L^{-1})) occurred on February 3, and the maximum occurred on October 6 (5.3×10^8 cell (L^{-1})). The minimum and maximum values of total phytoplankton abundance were 1.2×10^8 cell (L^{-1}) and 1.3×10^9 cell (L^{-1}), respectively. The fractional contribution of PCB to the total phytoplankton abundance is also shown in Fig. 8 (by the ordinate to the right). The fractional contribution of PCB to the total phytoplankton increases when the total phytoplankton abundance decreases. Note that the maximum fractional values (approximately 75%) occurred in the winter.

3.5. Relationship between salinity and PCB abundance

It is evident in Fig. 9, that at each station (R1–R6), PCB abundance (C) is proportional to salinity (S) in an approximately linear manner. Thus, change of PCB abundance (dC) is equal to the product of the change of salinity (dS) and gradient m (i.e. $m = dC/dS$). (Note that the gradient m is a depth related measure.) The constant of proportionality (or gradient m) varies for each station; the gradient was greatest for station R1 (river mouth) and the smallest value of the gradient occurred at the most upstream location (R6). This was true for summer (A, B), fall (C) and winter (D).

The total slope change (dm/dx) was defined as the difference between the gradients at stations R1 and R6 (i.e. $m_1 - m_6)/dx$ where dx is the distance between stations R1 and R6. The dependence of the total slope change on the river flow is presented in Fig. 10. Note that the dependence of the slope change upon Q is non-monotonic. For small values of Q (less than 282 $m^3\,s^{-1}$) the total slope change is positive; in contrast, the slope change is negative for larger Q. One interpretation of the small PCB concentrations in samples with low salinities is that cells are conservative tracers for sea water in the estuary. However, this may not be the complete explanation for a system which has other potential processes of loss (mortality; predation; variability of light, temperature, nutrients etc.) and advection. For the case of a system with strong advection there is insufficient time for cells to adapt to the changing environment, and so those cell counts are unchanged. This is the case for the Ebro estuary when it is stratified with a saline wedge. Flow rates, particularly at the mouth of the estuary, and also within the estuary, are very much greater compared to the upstream river flow rate when a saline wedge exists. This arises because mixing of fresh and sea water (in the estuary) results in much larger magnitudes of inflow and outflow at the mouth of the estuary (and also within the estuary) than the upstream river flow (Perkins, 1976). Effectively advection of salinity (and hence PCB abundance)

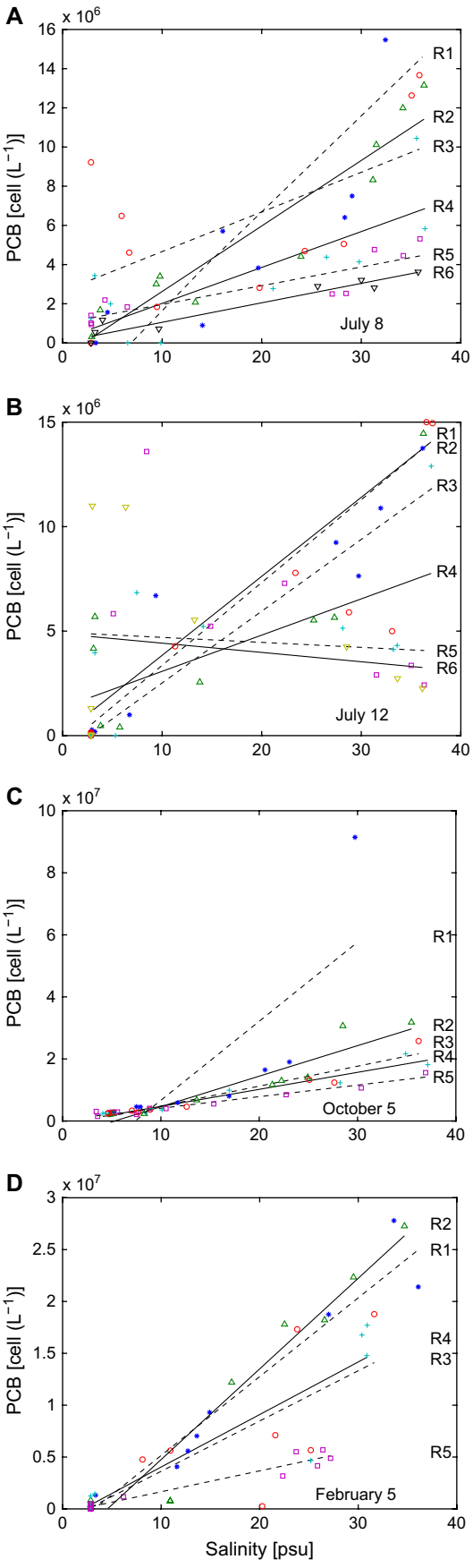

Fig. 9. Data for PCB against salinity from July 8 (A) and 12 (B), October 6 (C) and February 5 (D); lines are best-fit lines for cell–salinity gradient ($\partial C/\partial S = m$) through the data for each of the stations R1 (*, dashed), R2 (Δ, solid), R3 (○, dashed), R4 (+, solid), R5 (□, dashed) and R6 (▽, solid).

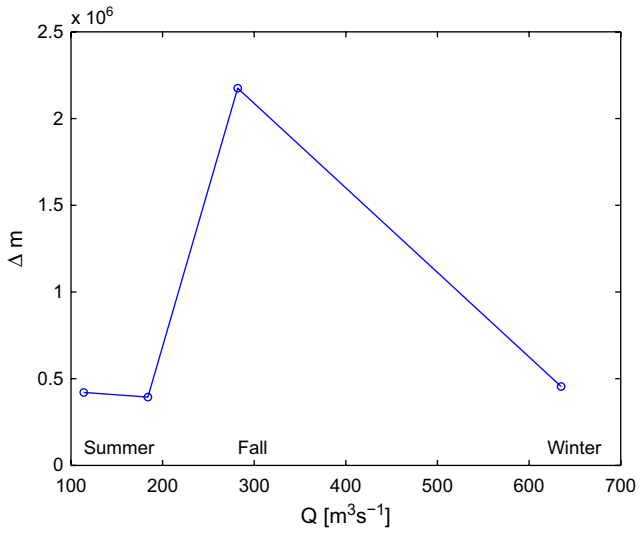

Fig. 10. Dependence of the total slope change (Δm) on flow rate Q.

dominates the other loss processes for large flow rates (in the winter months) in the Ebro estuary.

3.6. Analysis of PCB gradients

The maximum values of gradient (m_0) of PCB concentration occur at the mouth of the estuary: values decrease upstream. Fig. 11 shows the variation of the PCB gradient (m) through the estuary. The vertical axis is normalized by m_0 so as to yield a value of 1 for the normalized gradient at the river mouth. The horizontal axis is the upstream distance from the river mouth. It is evident that normalized gradients m/m_0 decrease with upstream distances to values of 0.15 at $x = 15$ km. The continual decrease of gradients is a characteristic of diffusive processes. The measured variations give a value of a diffusion coefficient of 1930 $m^2\,s^{-1}$. Hydrodynamic turbulent diffusion coefficients K_{hydro} can be calculated by estimating velocity and length scales of turbulent mixing; for this calculation, values of velocity and length scales are estimated to be proportional to mean velocity (0.5 $m\,s^{-1}$) and depth (10 m), so that an upper bound estimate of K_{hydro} is 5 $m^2\,s^{-1}$. The large value of 1930 $m^2\,s^{-1}$ is a biological turbulent diffusion coefficient K_{bio} for the decay of PCB is dominated by the losses of PCB. The ratio of K_{bio}/K_{hydro} is found to be given by:

$$K_{bio} = K_{hydro}\frac{1}{\log(\frac{m}{m_0})} \tag{4}$$

This shows that K_{bio} is equal to the product of K_{hydro} and a modulating factor proportional to $1/\log(m/m_0)$. This form

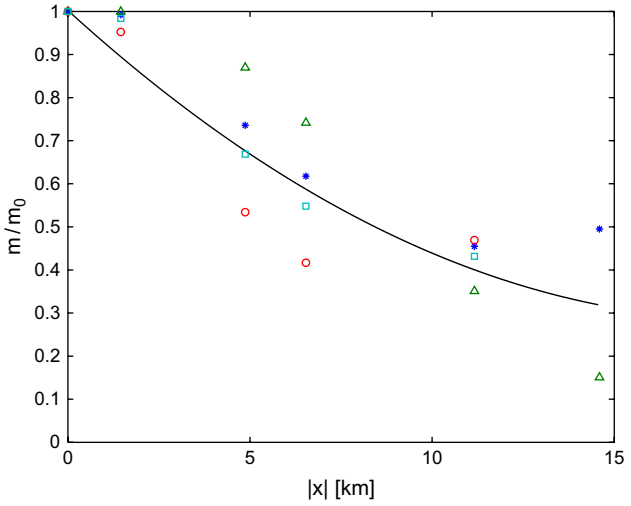

Fig. 11. Variation of normalized PCB cell number (m/m_0) with longitudinal distance x. Data for July 8 (*) and 12 (Δ), October 6 (○) and February 5 (□).

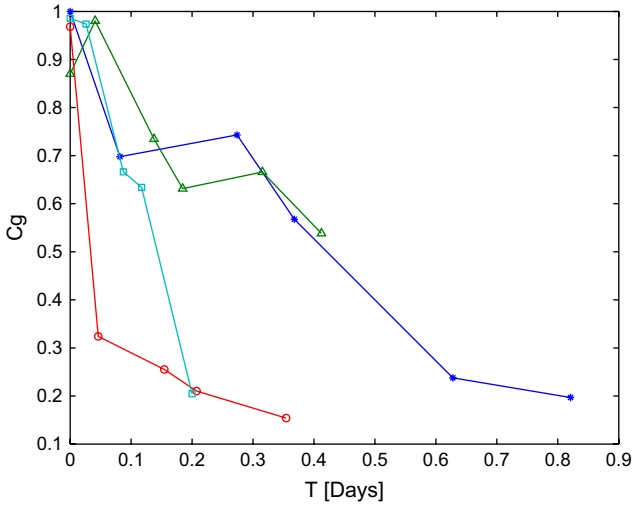

Fig. 12. Variation in the PCB cellular gradient (Cg) with time in the estuary. Data for July 8 (*) and 12 (Δ), October 6 (○) and February 5 (□). Cg values for winter decrease faster than in the summer.

of K_{bio} is consistent with the solution of the diffusion equation for a non-conservative scalar (Fischer et al., 1979).

4. Discussion

The Ebro estuary possesses a saline wedge, and the dynamics are dominated by the advection arising from mixing and large flow rates associated with a saline wedge. We find that inside the Ebro estuary the variations in PCB numbers can arise from salinity changes, and distance from the river mouth, or depend on the season. The present results are in accord with the general coastal and shelf ecosystem observations of PCB populations by Olson et al. (1990) and Chiang et al. (2002).

The Reynolds and the gradient Richardson numbers reflect hydrodynamic characteristics, and they can be utilized usefully, for example, to infer vertical mixing rates in a stratified estuary. It was noted previously that the value of the gradient m changes longitudinally from R1 to R6. We now show that the biological characteristics can be usefully described by a cellular gradient number (Cg) equivalent to a non-dimensional m. Cg is defined as

$$\mathrm{Cg} = \frac{\Delta S}{C_0}\frac{\mathrm{d}C}{\mathrm{d}S} \tag{5}$$

In Eq. (5) C_0 is the maximum cell number in the estuary, ΔS is the salinity range at a given R station, and $\mathrm{d}C/\mathrm{d}S$ is the gradient of PCB abundances with salinity (recall that $m = \mathrm{d}C/\mathrm{d}S$). By definition values of Cg can never be greater than 1.

Data for Cg variation are presented in Fig. 12, here the ordinate is the cellular gradient number (Cg) and the abscissa is the advection time ($T = x/u$). Values of Cg decrease from 1 to 0.15. There is a seasonal variation. Summer data for Cg decrease more slowly and approach values of 0.15 at $x/u \sim 0.9$. Winter and fall data for Cg decrease rapidly and approached values of 0.15 at $x/u \sim 0.3$. Note that lower flow rates in the summer increase advection times. (See Fig. 4 for flow rates.) This is accounted for by greater flow rates (and consequent greater turbulent diffusivities) in the winter and fall.

The data in Fig. 12 show that the values of Cg in the winter and fall decrease faster than in the summer, due to greater flow rates and advection. This is consistent with greater diffusivities. Large turbulent diffusivities increase mortality and the vertical transport of new PCB cells from saline waters to overlying fresher waters. The schematic of Fig. 13 shows the contrast between summer and winter scenarios. In summer, the fresh water flow rates are small ($<200\ \mathrm{m^3\ s^{-1}}$), and the interface is near horizontal at approximately 1 m depth from the surface, and values of Cg attenuate from the unity value (Cg ~ 1) at the mouth of the estuary to 0.15 at 11.5 km upstream by time $T = 19.2$ h. In winter, the fresh water flow rates are larger ($>600\ \mathrm{m^3\ s^{-1}}$) and the interface slopes to the bottom of the estuary; the range of values of Cg is similar (Cg ~ 1 at the mouth of the estuary and decreases to 0.15 at 15 km upstream by time $T = 8.6$ h).

The cellular gradient number evaluates the difference in abundance of PCB between the upper river water and the lower saline water in the estuary. As discussed previously, variations in Cg can rise from either hydrodynamic or biological effects, namely turbulent transport or losses (and/or growth), respectively. Our analysis showed that hydrodynamic turbulent diffusivities are approximately $5\ \mathrm{m^2\ s^{-1}}$ whereas biological turbulent diffusivities (inferred from Fig. 11) are $1930\ \mathrm{m^2\ s^{-1}}$; these are consistent with the greater role of losses in the estuary of the river Ebro. Note that we do not measure cell changes such as cell growth but rather consider cell numbers. In this work water samples were fixed to preserve the chlorophyll, and blue light was

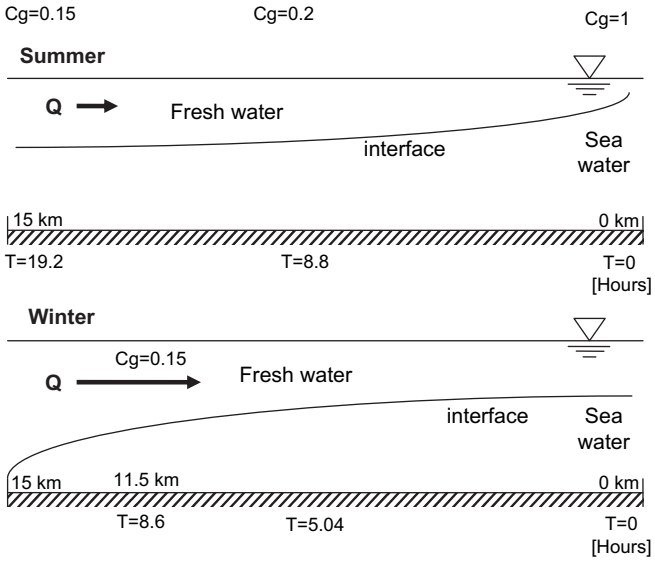

Fig. 13. Schematic of the evolution of the interface between the fresh water and sea water for the summer and winter. In the winter the flow rates are larger than in summer and the advection time for the interface to reach 15 km upstream is 8.6 h; this contrasts with advection time of 19.2 h in the summer. Values of Cg are 1.0, 0.2 and 0.15 at the mouth, 7.5 and 15 km upstream for both summer and winter.

used for cell counts under microscopy. This ensures that excited cells fluoresced whereas dead cells did not. This technique allows for the measurement of cell numbers in the water sample; however, we do not know the number of dead cells, or the cause of death.

Biologically the cellular gradient number, in this work can be interpreted as the ability of organisms (in our case PCB) to adapt to salinity changes in the aqueous environment. $Cg = 1$ implies perfect adaptation to changes in the environment, and equilibrium in population. $Cg \ll 1$ implies weak adaptability and large loss rates. Variations with salinity, specifically dC/dS, determine Cg values in the strongly advective and stratified Ebro estuary. We speculate that it will be possible to form equivalent Cg for other environmental variables such as temperature, light, nutrients and/or a combination of those can be important for other populations; we suggest that other such appropriately defined cellular gradient numbers will also be useful.

Acknowledgements

Field data surveys were supported by the European community, under the contract MAS3-CT98-0170 (DG12-VOMA); Preparation and Integration of analysis tools towards Operational forecast of Nutrients in Estuaries of European Rivers (PIONEER). We thank Dr. J. G. Del Río and the teams of U.P.V. and U.P.C. for their field assistance. Also the support during the Ph.D. studies for Alejandro Carrillo by the Mexican Consejo Nacional de Ciencia y Tecnología is gratefully acknowledged.

Appendix 1. List of variables and units

Variable	Definition	Variable	Definition
PCB	Picocyanobacteria	x	X direction
C	Cell number	y	Y direction
S	Salinity	z	Z direction
C_0	Maximum cell number in the estuary	D	Depth of the interface's beginning
Cg	Cellular gradient	h	Interface thickness
mS	Millisiemen	µ	Micron
m	Metre	Q	Flow
km	Kilometre	A	Area
°C	Celsius degree	u	Mean velocity
s	Second	N^2	Brunt Väisälä Frequency
°	Degree	Rig	Gradient Richardson number
′	Minute	ρ	Density
N	North	ρ_0	Mixing layer density
E	East	g	Gravity
mm	Millimetre	Re	Reynolds number
cm	Centimetre	ν	Kinematic viscosity
Hz	Hertz	Cell	Cells
%	Percentage	ml	Millilitre
×	Times	L	Litre
P	Probability		

References

Chiang, K.P., Kuo, M.C., Chang, J., Wang, R.H., Gong, G.C., 2002. Spatial and temporal variation of *Synechococcus* population in the East China Sea and its contribution to phytoplankton biomass. Continental Shelf Research 22, 3–13.

Fischer, H.B., List, E.J., Koh, R.C.Y., Imberger, J., Brooks, N.H., 1979. Mixing in Inland and Coastal Waters. Academic Press.

Ibáñez, C., Prat, N., Canicio, A., Curcó, A., 1999. El delta del Ebro, un sistema amenazado. Bakeaz, Bilbao.

Iriarte, A., 1993. Size-fractionated chlorophyll *a* biomass and picophytoplankton cell density along a longitudinal axis of a temperate estuary (Southampton Water). Journal of Plankton Research 15, 485–500.

Islam, M.S., Tanaka, M., 2004. Impacts of pollution on coastal and marine ecosystems including coastal and marine fisheries and approach for management: a review and synthesis. Marine Pollution Bulletin 48 (7–8), 624–649.

Lund, J.W.G., Kipling, C., Le Cren, E.D., 1958. The inverted microscope method of estimating algal numbers and the statistical basis of estimations by counting. Hydrobiologia 11 (2), 143–170.

Martínez, S., Rios, J., Pintó, J., Campos, A., 1999. Geografía. Teide, S.A., Barcelona.

Olson, R.J., Chisholm, S.W., Zettler, E.R., Altabet, M.A., Dusenberry, J.A., 1990. Spatial and temporal distributions of picoplankton in the North Atlantic Ocean. Deep-Sea Research 37, 1033–1051.

Pérez, M.C., Carrillo, J.A., 2005. Picocyanobacteria distribution in the Ebro Estuary (Spain). Acta Botanica Croatica 64 (2), 237–246.

Perkins, E.J., 1976. The Biology of Estuaries and Coastal Waters. Academic Press.

Raven, J.A., 1998. The twelfth Tansley Lecture. Small is beautiful: the picoplankton. Functional Ecology 12, 503–513.

Ray, T.R., Haas, L.W., Sieracki, M.E., 1989. Autotrophic picoplankton dynamics in a Chesapeake Bay sub-estuary. Marine Ecology Progress Series 52, 273–285.

Sieburth, J.M.N., Smatacek, V., Lenz, J., 1978. Pelagic ecosystem structure: heterotrophic compartments of the plankton and their relationship

to plankton size fractions. Limnology and Oceanography 23, 1256–1263.

Sin, Y., Wetzel, R.L., Anderson, I.C., 2000. Seasonal variations of size-fractionated phytoplankton along the salinity gradient in the York River estuary, Virginia (USA). Journal of Plankton Research 22 (10), 1945–1960.

Sournia, A., 1978. Phytoplankton manual. In: Monographs on Oceanographic Methodology 6. UNESCO, Paris, p. 337.

Turner, J.S., 1973. Buoyancy Effects in Fluids. Cambridge University Press.

Vargo, G.A., 1978. Using the fluorescence microscope. In: Sournia, A. (Ed.), Phytoplankton Manual. Monographs on Oceanographic Methodology. UNESCO, pp. 108–112.